Carbohydrate Polymers 240 (2020) 116325

Contents lists available at ScienceDirect

Carbohydrate Polymers

journal homepage: www.elsevier.com/locate/carbpol

Targeted delivery of honokiol by zein/hyaluronic acid core-shell nanoparticles to suppress breast cancer growth and metastasis

Qi Zhang[a,*], Jing Wang[a], Dan Liu[a], Wenquan Zhu[b], Shuang Guan[a], Li Fan[a], Defu Cai[a,*]

[a] Institute of Medicine and Drug Research, Qiqihar Medical University, Qiqihar, PR China
[b] College of Pharmacy, Qiqihar Medical University, Qiqihar, PR China

ARTICLE INFO

Keywords:
Nanoparticles
Zein
Hyaluronic acid
Honokiol
Breast cancer
Metastasis

ABSTRACT

Based on the antisolvent and electrostatic deposition methods, we fabricated zein/hyaluronic acid core-shell nanoparticles loaded with honokiol (HA-Zein-HNK), which could target delivery and enhance the therapeutic effect of the HNK. The prepared nanoparticles were found to have a mean size of 210.4 nm and negative surface charge. The HA-Zein-HNK nanoparticles exhibited improved antiproliferative and pro-apoptotic activities against 4T1 cells. Of note, the wound healing and transwell assessments indicated that the migration and invasion of 4T1 cells were markedly weakened by HA-Zein-HNK. Mechanistic insights revealed that HA-Zein-HNK downregulated the expressions of Vimentin and upregulated the expressions of E-cadherin. More importantly, an *in vivo* tissue distribution study demonstrated the excellent tumor target ability of HA-Zein. And these results correspond with the superior therapeutic efficacy of HA-Zein-HNK in 4T1 tumor bearing mice. In conclusion, we believe that HA-Zein nanoparticles may be served as a promising HNK delivery carrier for metastatic breast cancer therapy.

1. Introduction

Breast cancer is the most prevalent malignancies in women and does endanger women's lives and health worldwide (Siegel, Miller, & Jemal, 2019). At its early stage, breast cancer is a local disease, and can be controlled by surgery and radiation therapy (Chen et al., 2012). Unfortunately, it becomes aggressive and incurable once metastasis occurred. In fact, 90 % of breast cancer-related deaths for patients result from tumor metastasis (Liang et al., 2017). At present, traditional chemotherapy is still the first choice for clinical metastatic breast cancer treatment. However, low concentrations of chemotherapeutic drugs at the tumor site make them unable to effectively control and treat the tumor. At the same time, many of these chemotherapeutic drugs often cause unsatisfactory outcomes and severe systemic side effects as their rapid clearance from systemic circulation and similar cytotoxicity to both cancerous and healthy cells (Zhang et al., 2019).

The introduction of nanotechnology in drug delivery systems (DDS) provides new ideas to overcome these drawbacks. The nanosized DDS can be passively or actively enriched in tumor tissues, taking advantage of the enhanced permeability and retention (EPR) effects in solid tumors and the high affinity of ligands/antibodies for corresponding receptors overexpressed on tumor cells (Lang et al., 2017). In addition, the nanosized DDS have been successfully used to improve the solubility and chemical stability of antitumor drugs. Traditional materials such as synthetic polymers and inorganic materials have been widely applied for nanosized DDS. However, several limitations including complicated synthesis procedures, less available and severe *in vivo* toxicity still limit their application (Seok et al., 2018). Therefore, naturally-derived biopolymers have drawn significant attention as they possess important properties including biocompatibility, biorenewability, and sustainability (Sheikhi et al., 2019).

Zein, a naturally occurring amphiphilic protein from corn, possesses many proven advantages such as biodegradability, biocompatibility, non-toxicity, low cost, and easy availability. As a GRAS material for human use, zein has been used as an ideal material in the food industry and drug delivery for many years (Jiang et al., 2019; Zhang, Cui et al., 2015). Indeed, it has been reported to apply in a variety of formulations, such as micro/nanoparticles, nanofibres, film coatings, powders, and nanogels (Kaushik, Rawat, Aswal, Kohlbrecher, & Bohidar, 2019; Tran, Dian, Lee, & Tran, 2019). Of note, zein has been widely used to prepare protein nanoparticles that are able to encapsulate and deliver various bioactive molecules (Chen, Han, Huang et al., 2019). However,

* Corresponding authors at: Institute of Medicine and Drug Research, Qiqihar Medical University, NO. 333, Bukui Street, Jianhua Distict, Qiqihar, Heilongjiang Province 161006, PR China.
E-mail addresses: zhangqi@qmu.edu.cn (Q. Zhang), wangjing@qmu.edu.cn (J. Wang), liudan@qmu.edu.cn (D. Liu), Zhuwq@qmu.edu.cn (W. Zhu), 2362459435@qq.com (S. Guan), Fanli@qmu.edu.cn (L. Fan), cai@qmu.edu.cn (D. Cai).

https://doi.org/10.1016/j.carbpol.2020.116325
Received 14 February 2020; Received in revised form 5 April 2020; Accepted 15 April 2020
Available online 28 April 2020

zein nanoparticles often exhibit poor physicochemical stability against aggregate and precipitate when exposed to acid, base, high salt content, and high temperatures (Chen, Han, Wang et al., 2019). In contrast to individual zein nanoparticles, zein and other natural materials complex have excellent physicochemical stability. The complexes formed between zein and other natural materials are easy to fabricate, which convey advanced features to zein-based delivery systems (Li et al., 2018).

In this context, hyaluronic acid (HA) is another naturally occurring biopolymer made up of multiple disaccharide units of *N*-acetyl-D-glucosamine and D-glucuronic acid (Ganesh, Iyer, Morrissey, & Amiji, 2013). HA is a biocompatible polysaccharide with many physiological functions, such as anti-aging, anti-inflammation, angiogenesis, and embryonic development (Dicker et al., 2014). Owing to its outstanding hydrophilicity, biodegradability, biocompatibility, non-toxic and non-immunogenic nature, and target ability to CD44 receptors over-expressed in tumor cells, HA possesses great potential in biomedical and pharmaceutical applications (Dosio, Arpicco, Stella, & Fattal, 2016; Wang, Liu et al., 2020). The incorporation of HA into nanosized DDS has previously been shown to improve their drug retention, serum stability and delivery profiles (Pulakkat, Balaji, Rangarajan, & Raichur, 2016). Thus, the complex between HA and zein would be highly beneficial for therapeutic agents treating deadly diseases like cancer (Seok et al., 2018).

Honokiol (HNK), a vital bioactive biphenolic compound found in Magnolia, exerts multiple biological functions including anti-inflammatory, antioxidant, antidepressant, anticancer and neuroprotective properties (Wang, Liu et al., 2020; Xu et al., 2019). Recent studies have demonstrated that HNK can suppress the growth and metastasis of a wide variety of tumors such as those of the brain, breast, colon, liver, lung and skin malignancies (Banik et al., 2019). The underlying regulatory mechanisms that HNK on tumor metastasis have been elucidated through the modulation of matrix metalloproteinase, PI3K/Akt/mTOR, epithelial to mesenchymal transition, NF-κB, STAT3, and Wnt signaling pathways (Chiu et al., 2019; Wang, Shang, Li, & Chen, 2019). However, the use of HNK in tumor treatment is limited due to its poor water solubility and low bioavailability (He et al., 2020; Zhang, Chen et al., 2015). Thus, a formulation consisting of HA and zein would be very beneficial to delivery HNK enhancing its solubility, bioavailability and subsequently its inhibitory effect against breast cancer.

In previous studies, only little information focused on HA and zein based nanosized DDS, there was no research on zein/HA core-shell nanoparticles so far. Therefore, the main aim of our study was to physically coat HNK-loaded zein nanoparticles (core) with hydrophilic HA (shell), which would endow them with selective cellular uptake and much higher stability *in vivo* (Scheme 1). We hypothesized that cationic zein nanoparticles could easily be coated with anionic HA forming core-shell nanoparticles, which would be used to load the hydrophobic HNK antitumor agent through hydrophobic effect and hydrogen bonding. And another hypothesis was that the HNK loaded zein/HA core-shell nanoparticles (HA-Zein-HNK) would improve the *in vivo* biodistribution and enhance suppression of breast cancer growth and metastasis for HNK, which would be achieved by protecting the HNK molecules within the core of nanoparticles and targeting delivery mediated by HA/CD44. Thus, the present work involved the fabrication, characterization and *in vitro* and *in vivo* evaluation of novel HA-Zein-HNK nanoparticles to enhance suppression of breast cancer growth and metastasis. It was expected that the HA-Zein-HNK would provide a promising strategy of efficient therapy for breast cancer metastasis.

2. Materials and methods

2.1. Materials

HNK (> 98 %) was obtained from Meilun Biotechnology Co., Ltd. (Dalian, China). Zein (> 98 %) and Tween 80 were purchased from J&K Scientific Ltd. (Beijing, China). HA (with MW of 10, 140 and 980 kDa) were produced by Zhenjiang Dong Yuan Biotech Co., Ltd. (Zhenjiang, China). Sulforhodamine B sodium salt (SRB), matrigel, coumarin-6 (Cou6), and Hoechst33258 were all purchased from Sigma-Aldrich (Shanghai, China). Annexin V-FITC/PI apoptosis detection kit was purchased from ComWin Biotech Co., Ltd. (Beijing, China). Rabbit polyclonal anti-human-Bcl-2, mouse polyclonal anti-human-Bax, rabbit polyclonal anti-GAPDH, rabbit anti-mouse immunoglobulin G (IgG) and goat anti-rabbit IgG were all obtained from Cell Signaling Technology (Danvers, USA). Rabbit polyclonal antibodies against E-cadherin and Vimentin were purchased from Proteintech (Chicago, USA). RPMI-1640 medium and penicillin-streptomycin were obtained from M&C Gene Technology LTD. (Beijing, China). Fetal bovine serum (FBS) was produced by Wisent Co., Ltd (Nanjing, China).

2.2. Cell culture and animals

4T1 murine mammary carcinoma cells were purchased from the Institute of Basic Medical Science, Chinese Academy of Medical Sciences (Beijing, China). The cells were maintained in RPMI-1640 medium supplemented with 10 % FBS and 100 IU/mL penicillin and 100 μg/mL streptomycin. All cells were cultured in a humidified incubator at 37 °C in 5 % CO_2 air. Female BALB/c mice of 18–20 g were obtained from Liaoning Experimental Animal Resource Center (Benxi, China). All animal procedures were performed under protocols approved by the Ethical Committee of Qiqihar Medical University.

2.3. Preparation and characterization of HNK-loaded zein/HA core-shell nanoparticles

The nanoparticles were obtained by the antisolvent precipitation and electrostatic deposition methods with some modifications as described previously (Hu & McClements, 2015). Briefly, zein (100 mg) and HNK (10 mg) were dissolved in a 5.0 mL aqueous ethanol solution (70 %, v/v) with stirring at 1000 rpm for 1 h to complete dissolve. And this mixture was adjusted to pH 5.7 using 1 mol/L HCl. Then, a volume of 5.0 mL zein-HNK solution was rapidly dropped into 20.0 mL 0.05% Tween 80 solution (adjusted to pH 4.0) with constant stirring at 1000 rpm for 30 min. The remaining ethanol was evaporated from the prepared nanoparticles suspension at 37 °C using a rotary evaporator (RE100-Pro, Beijing DLAB Scientific Co., Ltd, China). The samples prepared at this step are referred to as Zein-HNK nanoparticles. The prepared Zein-HNK nanoparticles suspension (5.0 mL) was poured into 5.0 mL 0.05% HA (adjusted to pH 4.0) aqueous solution with stirring at 1000 rpm for 1 h. The resulting samples were HNK loaded zein/HA core-shell nanoparticles and referred to as HA-Zein-HNK. Finally, the HA-Zein-HNK was washed twice by centrifugation at 12,000 rpm to remove non-entrapped HNK, Tween 80 and free HA. To construct nanoparticles loaded with Cou6 or DiR, the prepared steps were the same as those mentioned above except that the HNK was substituted with Cou6 or DiR.

The structures and morphologies of the nanoparticles were analyzed using a transmission electron microscopy (TEM, JEOL JEM-1200EX, Japan). A 10 μL diluted nanoparticles sample was placed on a copper grid, followed by negative staining using 2 % uranyl acetate. After air dried at room temperature, the samples were observed with the TEM instrument operating at 100 kV. The mean particle diameter, polydispersity index (PDI) and zeta-potential values of various nanoparticles were determined using the dynamic light scattering (DLS) technique and a Nicomp 380ZLS Particle Sizing System (PSS, USA). The encapsulation efficiency (EE) of HNK in nanoparticles was analyzed by a Waters UPLC system including sample manager-FTN, quaternary solvent manager, and DAD detector. The separation was performed on a Waters BEH-C18 column (2.6 mm × 100 mm, 1.7 μm) operated at 30 °C. The mobile phase was a 70: 30 v/v mixture of acetonitrile and water at a flow rate of 0.35 mL/min. The HNK was detected at 294 nm.

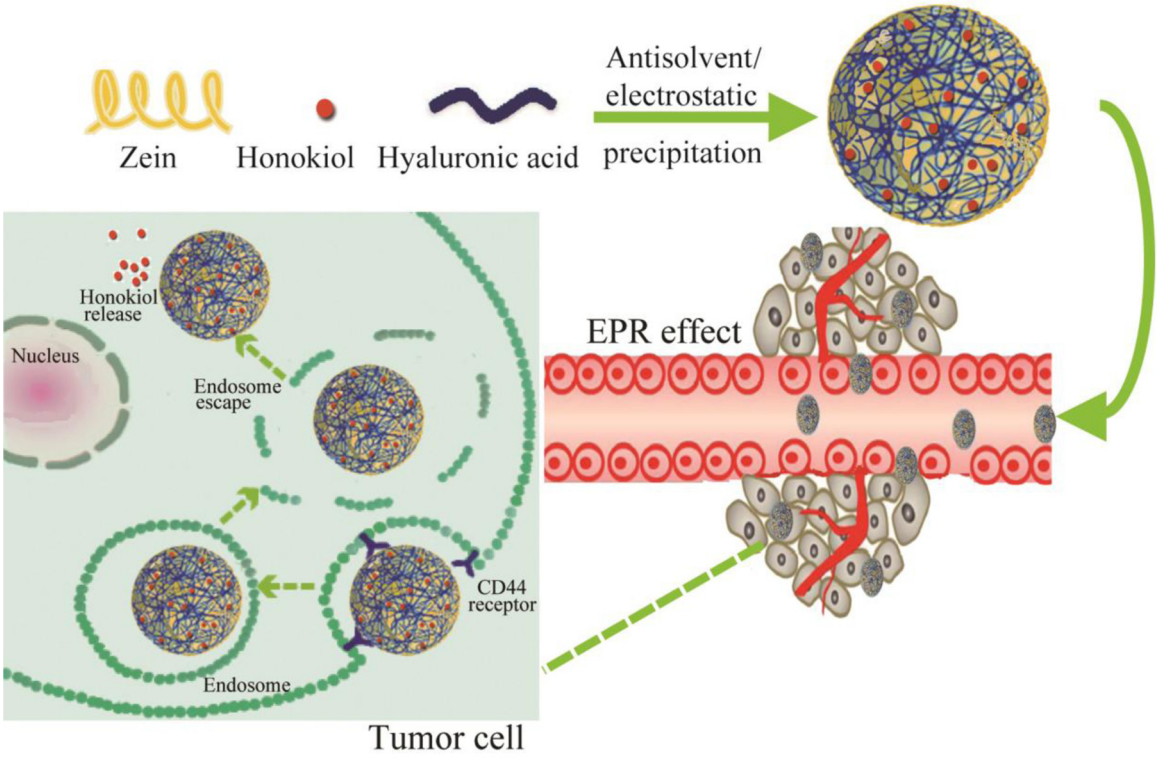

Scheme 1. Graphic illustration of the preparation strategy and the antitumor function of HA-Zein-HNK nanoparticles.

The EE was calculated by the following expression: EE = $W/W_0 \times 100$ %, where W_0 and W represent the measured amount of HNK in the nanoparticles before and after centrifugation, respectively.

In order to verify the serum stability of nanoparticles during body circulation, the stability test was investigated in PBS containing 50 % FBS by measuring the mean size and PDI changes. The nanoparticles of Zein-HNK and HA-Zein-HNK were placed into PBS containing 50 % FBS with shaking at 150 rpm and 37 °C. At each specific time point, 100 μL of sample was collected for the particle size and PDI measurements by Nicomp 380ZLS Particle Sizing System (PSS, USA).

Release behaviors of HNK from free HNK, Zein-HNK and HA-Zein-HNK were assayed using the dialysis diffusion method *in vitro*, which was carried out in PBS (pH 7.4) with 0.2 % Tween 80. In total, 1 mL of each formulation was transferred into a dialysis bag (MWCO = 12000–14000 Da), respectively. Then the sealed dialysis bags were dialyzed against 30 mL of release medium with horizontal oscillation at 37 °C and 100 rpm. At selected time points, 1 mL of release medium was collected, and an equal volume of fresh medium was added. The released HNK in the outside medium was measured *via* HPLC over 48 h.

2.4. In Vitro cellular uptake and HA competition assay

The cellular uptake of HA-Zein nanoparticles was performed in 4T1 cells by loading Cou6 into the particles to monitor Cou6 fluorescence using flow cytometry and confocal imaging. 4T1 cells were placed in 6-well plates (1×10^5 cells/well) and cultured for 24 h under the condition of 5 % CO_2 at 37 °C. After washed twice with PBS, the cells were treated with Zein-Cou6, HA-Zein-Cou6 and free Cou6 in serum-free medium for 1 h (Cou6: 100 ng/mL). The cells were washed three times with cold PBS to end the uptake. Then, the cells were trypsinized, centrifuged and re-dispersed in 0.5 mL PBS. Cellular uptake of Cou6 was measured by a FACScan flow cytometer (BD FACSCalibur, USA) with the cells collected 1×10^4. A receptor competitive assay was designed to evaluate whether the HA-Zein nanoparticles were specifically transferred into the 4T1 cells through HA/CD44 receptor endocytosis, an addition of free HA (2.0 mg/mL) was added to the cell for 1 h prior to the HA-Zein-Cou6 treatment.

For the confocal microscopy study, 4T1 cells were cultured into glass-bottom dishes and processed as described above. After 1 h of uptake, the cells were washed three times with cold PBS, followed by fixed with 4% paraformaldehyde for 20 min and cell nuclei stained with Hoechst 33,258 for another 20 min. Finally, an LSM710 laser confocal microscope (Zeiss, Germany) was used to observe and analyze the fluorescent signals in 4T1 cells.

2.5. In vitro cytotoxicity and apoptosis assay

The SRB colorimetric method was used to evaluate the *in vitro* cytotoxicity of various HNK formulations. The 4T1 cells at the exponential phase were seeded into 96-well plates at 2×10^3 cells/well for 24 h. The cells were treated with different Zein-HNK, HA-Zein-HNK and free HNK solutions, to give final HNK concentrations ranging from 0.30 to 20 μg/mL. After further culture for 48 h, the cells were fixed with 10% cold trichloroacetic acid, dried in the air, and stained with 0.4% SRB dye. Subsequently, 150 μL Tris base solution (10 mM) was added to dissolve the SRB dye. Finally, the optical densities representing cell viability were determined by a plate reader (Tecan Safire2, Switzerland) at 540 nm.

Moreover, the cell apoptosis was analyzed by an AnnexinV-FITC/PI staining and a flow cytometry analysis. In brief, 4T1 cells seeded into the 6-well plates were treated with Zein-HNK, HA-Zein-HNK and free-HNK for 24 h. All HNK-loaded formulations contained the equivalent HNK concentration of 5 μg/mL. Untreated cells were used as the negative control. Harvested cells were washed twice with PBS, and re-dispersed in 300 μL binding buffer. Finally, the cells were stained with Annexin V-FITC and PI for 15 min away from light and subjected to analysis using a FACScan flow cytometer.

2.6. In vitro cell migration and invasion test

Wound healing, transwell migration and invasion assays were carried out to assay the inhibitory effect of HA-Zein-HNK on cell migration and invasion capacities. For the wound healing assay, 4T1 cells were cultured in 6-well plates and allowed to attain 70–80 % confluence. Then a straight wound was gently scratched with a sterile 200 μL pipette tip, followed by washing with PBS to remove floating cells. Subsequently, the cells were incubated with Zein-HNK, HA-Zein-HNK and free-HNK at equivalent HNK dose of 5 μg/mL. Cell migration was monitored over 24 h using an inverted microscope (Zeiss, Axio Observer A1). The wound healing rate was calculated as previously described (Zhang et al., 2014).

For transwell migration and invasion assays, transwell chambers (Costar, Cambridge, USA) with 8-μm pore polycarbonate filters were used. In brief, 4T1 cells were pretreated with various HNK formulations at a concentration of 5.0 μg/mL HNK. After 24 h incubation, the cells were trypsinized and suspended in serum-free RPMI-1640 medium. And 100 μL cell suspension containing 5×10^4 cells for migration or 8×10^4 cells for invasion were seeded into the upper chambers coated without or with 50 μL of Matrigel (Corning, USA). The RPMI-1640 medium containing 10% FBS was placed in the lower chamber. After incubation for 24 h (or 36 h for invasion), the non-migratory cells on the top chamber were removed with cotton swabs. The cells attached to the bottom of the membrane were fixed with 4 % paraformaldehyde, stained with 0.4 % crystal violet for 30 min, and observed under an inverted microscope (Zeiss, Axio Observer A1). Later, the stained cells were washed with 33% acetic acid to detach the crystal violet into an empty well. The number of invaded cells was determined by measuring the absorbance of the crystal violet solution at 570 nm. Finally, the percentages of migratory and invasive cells were calculated according to the absorbance value.

2.7. In vitro western blotting analysis

Western blotting was used to detect the expressions of apoptosis and migration related proteins. 4T1 cells were pretreated with Zein-HNK, HA-Zein-HNK and free HNK at HNK concentration of 10 μg/mL for 24 h. Cells were harvested and lysed. The proteins from cell lysates were quantified used the BCA Protein Assay Kit (Beyotime, China). Afterwards, the proteins were resolved by SDS-PAGE and electroblotted onto nitrocellulose membranes (Millipore, MA, USA). Then the blotted membranes were incubated with primary antibodies, followed by incubation with secondary antibodies conjugated with horseradish peroxidase (Beyotime, China) (Lv, Qiao, Su, & Chen, 2016). Protein bands were visualized with the enhanced chemiluminescene (ECL) detection under the ChemiDoc™MP imaging system (Bio-Rad, USA).

2.8. Inhibitory effect on the tumor spheroids

The hanging-drop method was utilized to culture 4T1 multicellular tumor spheroids as established previously (Del Duca, Werbowetski, & Del Maestro, 2004). Typically, the agarose-coated 48-well plate was prepared in advance with 2 % agarose to provide a non-adherent surface. Then, about 1000 4T1 cells in 20 μL of culture medium droplets were hanged onto the inner surface of the lid of a 48-well plate. After 48 h, the formed tumor spheroids were transferred to each well containing complete RPMI-1640 medium for further culture. The media was refreshed every two days until spheroids grew to 400–500 μm. Then the tumor spheroids were exposed to free HNK, Zein-HNK and HA-Zein-HNK at an equivalent concentration of HNK (10 μg/mL), respectively. The growth inhibition assay was monitored by observing the morphology and size of the spheroids under an inverted microscope (Zeiss, Axio Observer A1).

2.9. In vivo tissue distribution of DiR-loaded NPs by living imaging

To construct a tumor-bearing mouse model, female BALB/c mice were subcutaneously injected with 1×10^6 4T1 cells/mouse into the right armpit. When the tumor volume reached approximately 300–400 mm^3, the animals were allocated at random into three groups (3 per group). Mice were intravenously treated with 0.1 mL of free DiR, Zein-DiR and HA-Zein-DiR (DiR: 500 μg/kg) *via* the tail vein. Thereafter, the mice were anesthetized with isoflurane at different time points following administration and photographed using an *in vivo* imaging system (IVIS Lumina Series III, PerkinElmer, USA). At the end of the *in vivo* imaging, the mice were sacrificed by cervical dislocation to dissect and collect tumors and other major organs. The *ex vivo* fluorescence images for all dissected organs were also obtained.

2.10. In vivo therapeutic efficacy and toxicity studies

The therapeutic efficacy was evaluated with the 4T1 tumor bearing BALB/c mice as established above. On the 9th day after inoculation, the mice were randomly divided into four groups. After that, the mice in different groups were administered with the following four formulations *via* tail vein injection respectively: physiological saline, Free HNK, Zein-HNK and HA-Zein-HNK. The drug administration was performed every 2 days for a total of 4 times at HNK equivalent dosage of 15 mg/kg. The mice were then measured every other day for tumor volumes and body weights. On day 15 after the tumor inoculation, the mice were sacrificed and the major organs and tumors were collected. Then the tumors were weighed and took pictures. The expression of Bcl-2 and Bax in the tumor was measured by Western blotting as described above. The tissue sections were prepared for the pathology analysis by hematoxylin and eosin (H&E) staining. After 48 h of fixation in Bouin's fluid, the numbers of metastatic nodules on isolated lungs were counted to assess the antimetastasis efficacy. To evaluate the apoptosis of tumor cells histologically, the tumor sections were further detected with a fluorometric TUNEL apoptosis detection kit (Promega, USA) according to the manufacturer's instructions, followed by examination under an LSM710 laser confocal microscope.

2.11. Statistical analysis

All experiments were performed at least in triplicate and all data were presented as the mean ± standard deviation. Statistical differences were determined by one-way ANOVA, followed by Student's non-paired *t*-test. The differences were considered statistically significant for data with p-value < 0.05, and very significant for data with p-value < 0.01.

3. Results and discussions

3.1. Preparation and characterization of HNK-loaded zein/HA core-shell nanoparticles

Initially, the influence of HA molecular weight on the physicochemical properties of the zein nanoparticles was investigated. 140 kDa HA exerted the best dispersion and stability for zein nanoparticles compared with 10 kDa and 980 kDa HA. Thus, 140 kDa HA was applied in the subsequent research. As illustrated in Fig. 1A, pure Zein-HNK nanoparticles had a mean diameter of 159.7 nm and a slightly turbid appearance confirming that small zein nanoparticles were prepared. Most of the zein nanoparticles aggregated and formed visible sediments when either 0.005 % or 0.01 % HA was added into these nanoparticles. However, after increasing HA concentration further to 0.015 %, the particle size decreased significantly and then leveled off at about 210.4 nm for HA concentrations of 0.025 % or higher. When HA molecules were too few to completely cover the surfaces of zein nanoparticles (*e.g.*, 0.005 % and 0.01 % HA), a large number of sediments

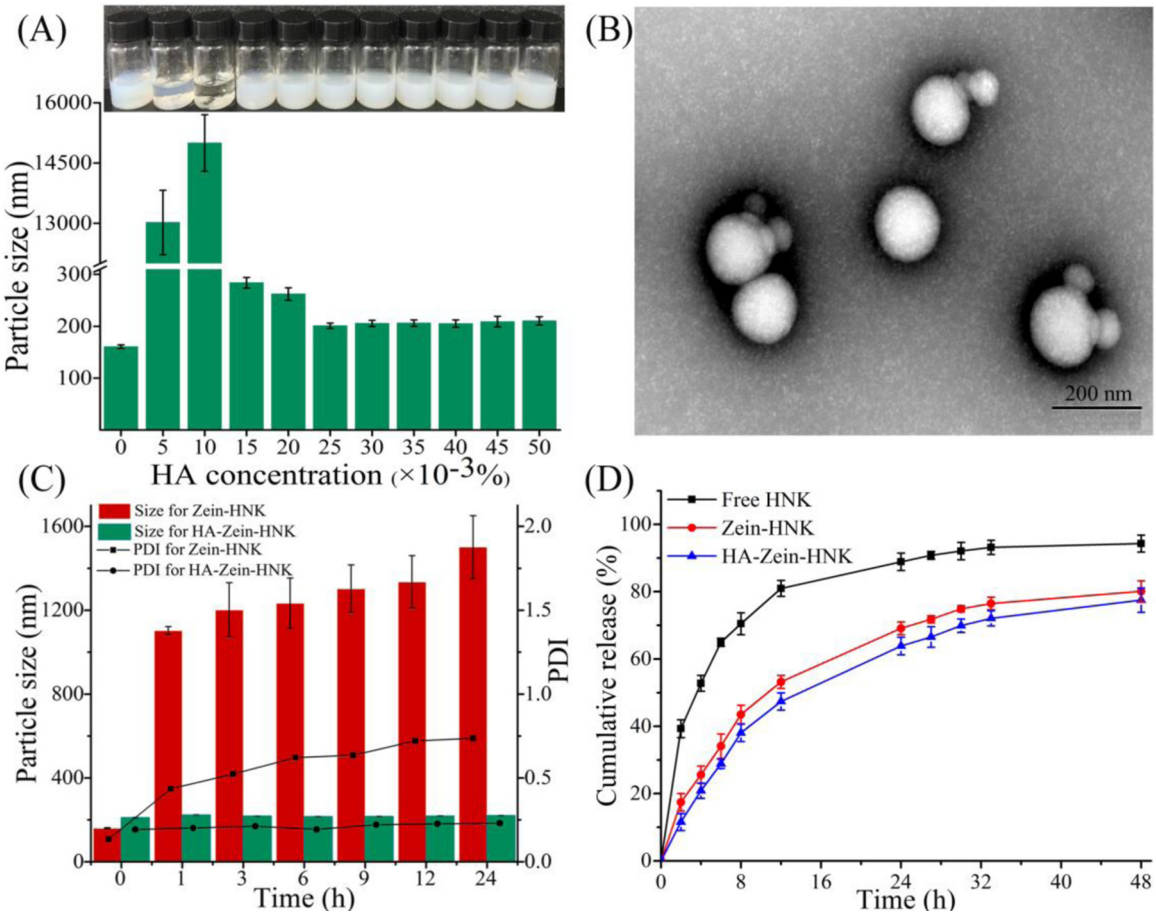

Fig. 1. Characterization of the HA-Zein-HNK. (A) The representative images and particle sizes of HA-Zein-HNK at different HA concentrations. (B) TEM image of HA-Zein-HNK nanoparticles. (C) Stability studies of HA-Zein-HNK and Zein-HNK after incubation in PBS containing 50 % FBS at 37 °C for 24 h. (D) The *in vitro* cumulative HNK release at 37 °C during 48 h. Data are shown as mean ± SD (n = 3).

would appear due to the reduction of electrostatic repulsion and bridging flocculation. However, the surfaces of zein nanoparticles would be thoroughly covered with a layer of HA molecules at higher HA concentrations (*e.g.*, > 0.015 % HA), which rendered the nanoparticles stable as the combination of electrostatic and steric repulsion. A similar trend was reported for alginate-zein nanoparticles, where the particle size increased first and then decreased as the alginate amount was raised (Hu & McClements, 2015). The zeta-potential of pure Zein-HNK was +18.66 ± 1.6 mV, however, the zeta-potential of HA-Zein-HNK was converted to -34.54 ± 2.8 mV. This change in surface charge property of HA-Zein-HNK implied that anionic HA molecules coated onto the surfaces of cationic Zein-HNK nanoparticles by electrostatic adsorption. It was widely known that a particulate solution is considered colloidally stable if the value of the zeta potential is above 30 mV or below −30 mV (Li et al., 2018). The TEM picture showed in Fig. 1B demonstrated that the optimized HA-Zein-HNK was spherical in morphology and had a uniformly distributed particle size of around 200 nm with a narrow PDI value. It was worth noting that a close core-shell structure was formed between zein and HA. All the zein nanoparticles exhibited high EE for HNK, and the EEs were in a range of 88.1 %–93.6 %.

Particle size, as one of the most important parameters, was often used to explore the stability of nanoparticles (Song et al., 2019). As shown in Fig. 1C, the particle size and PDI of HA-Zein-HNK in PBS containing 50 % FBS did not change significantly over 24 h, while the particle size and PDI of Zein-HNK increased sharply in the presence of serum. This phenomenon may have been because of the presence of hydrophilic HA, thereby providing a protective barrier in the outer layer of zein nanoparticles. This stereospecific blockade could avoid the accumulation of nanoparticles and attenuating the recognition and destruction of nanoparticles by plasma components, thus making the nanoparticles more stable (Peer & Margalit, 2004).

The release profiles of HNK from free HNK, Zein-HNK and HA-Zein-HNK are shown in Fig. 1D. Compared to free HNK solution, Zein-HNK and HA-Zein-HNK nanoparticles exhibited slow sustained release process. Both formulations exhibited a biphasic pattern characterized with fairly rapid release during the initial period and followed by a slow release over 48 h. At the first 2 h, Zein-HNK and HA-Zein-HNK nanoparticles released about 17.4 % and 11.6 % of HNK, respectively. And nearly 80.1 % of HNK was released from Zein-HNK over 48 h, while the cumulative release of HNK in HA-Zein-HNK was 77.5 %, indicating that the existence of HA slightly slowed down the release rate of HNK. HA is a kind of strong hydrophilic polysaccharide. When the nanoparticles are coated around by HA, HA molecules swell and form a dense hydration layer around the nanoparticles in aqueous solution, which will shield the drug release (Ravar et al., 2016).

3.2. Cellular uptake and HA competition assay

To determine the role of HA and CD44 in enhanced cellular uptake, we first investigated the cellular uptake by flow cytometry. In this study, Zein and HA-Zein nanoparticles were labeled with a green fluorescent probe of Cou6. As shown in Fig. 2A and B, the order of the mean fluorescence intensities was control < Zein-Cou6 < HA + HA-Zein-Cou6 < HA-Zein-Cou6 < free Cou6. HA-Zein-Cou6 (68.5 ± 3.98) exhibited the higher cellular uptake than Zein-Cou6

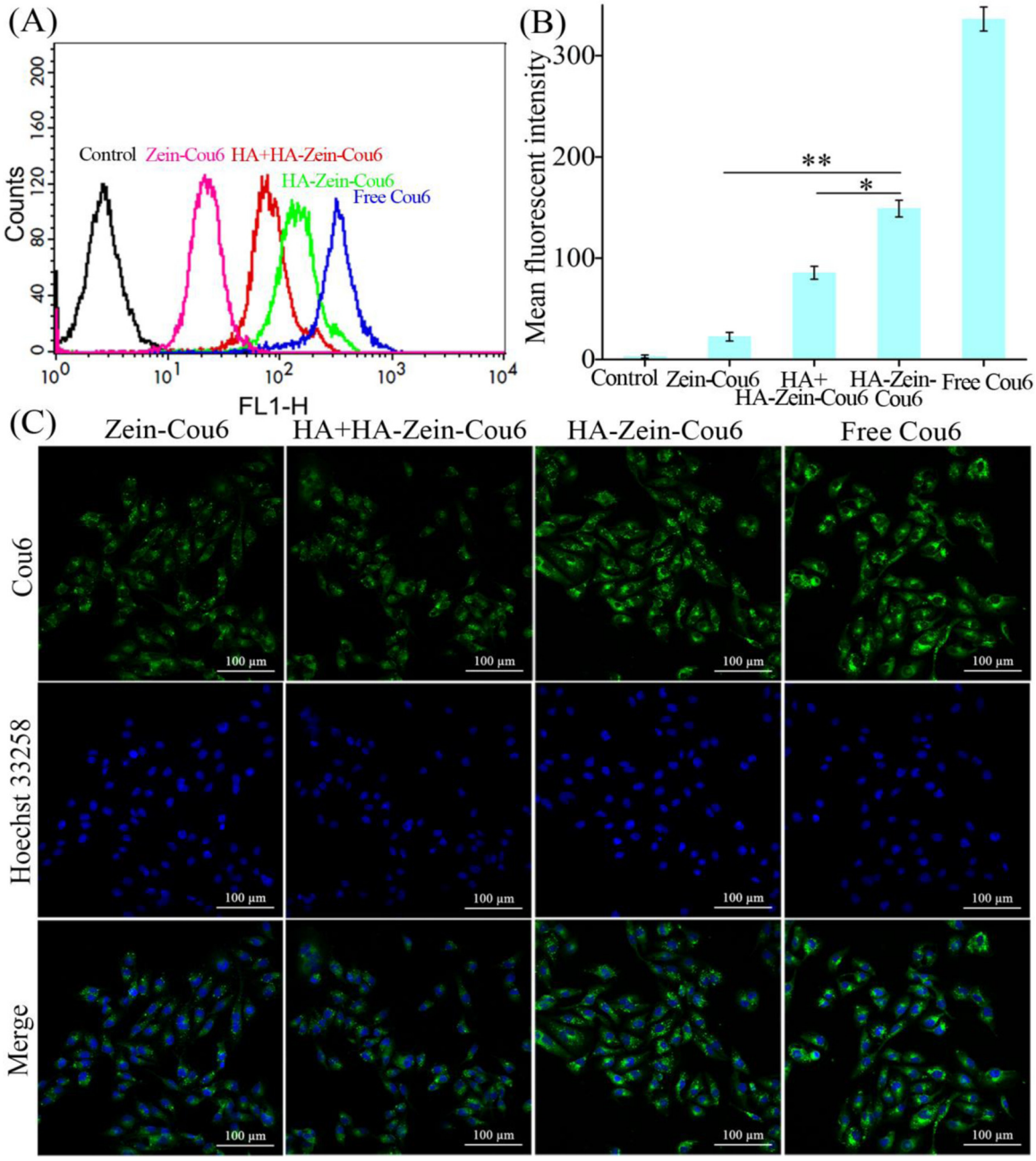

Fig. 2. Intracellular uptake study of Zein-Cou6, HA + HA-Zein-Cou6, HA-Zein-Cou6 and free Cou6 on 4T1 cells after incubation for 1 h at 37 °C. (A) Flow cytometric quantitative determination of Cou 6 uptake. (B) Quantitative analysis of Cou6 uptake based on flow cytometric plots. Each bar represents the mean fluorescence intensity ± SD ($n = 3$), *$p < 0.05$, **$p < 0.01$. (C) Intracellular distribution of nanoparticles was observed by laser scanning confocal microscopy. Green and blue indicate the fluorescence of Cou6 and Hoechst 33,258, respectively. (For interpretation of the references to colour in this figure legend, the reader is referred to the web version of this article).

(22.4 ± 3.26), implying that HA-CD44 mediated endocytosis had more contribution to enhanced uptake of HA-Zein-Cou6 than electronic adsorption effect. Moreover, after saturation of CD44 receptor with HA, the cellular uptake of the HA-Zein-Cou6 was significantly reduced. This phenomenon clearly indicated that the 4T1 cells endocytosis of HA-Zein-Cou6 was greatly facilitated by the CD44-mediated internalization.

In an effort to shed more light on the cellular uptake, confocal laser scanning microscopy was performed for Cou6-loaded nanoparticles (Fig. 2C). The results are quite in line with flow cytometry. In comparison with Zein-Cou6 group, a more intense fluorescence signal was observed in 4T1 cells incubated with HA-Zein-Cou6. However, the enhanced intracellular fluorescence intensity was reversed by pre-incubation with excess of free HA (HA + HA-Zein-Cou6). These results indicated that HA-modifying enabled zein nanoaprtilces to target 4T1 cells through the CD44 receptor.

3.3. In vitro cytotoxicity and apoptosis assay

SRB assay was used to detect the *in vitro* anti-cancer ability of various HNK formulations. As shown in Fig. 3A, significant cytotoxicity of Zein-HNK, HA-Zein-HNK and free HNK in 4T1 cells was observed, and IC_{50} values were calculated to be 10.05 ± 1.19, 4.84 ± 0.74 and 2.36 ± 0.85 μg/mL, respectively. It was obvious that free HNK, a positive control, exhibited stronger cytotoxicity than the two HNK-loaded zein nanoparticles. Under the *in vitro* condition, free HNK could directly

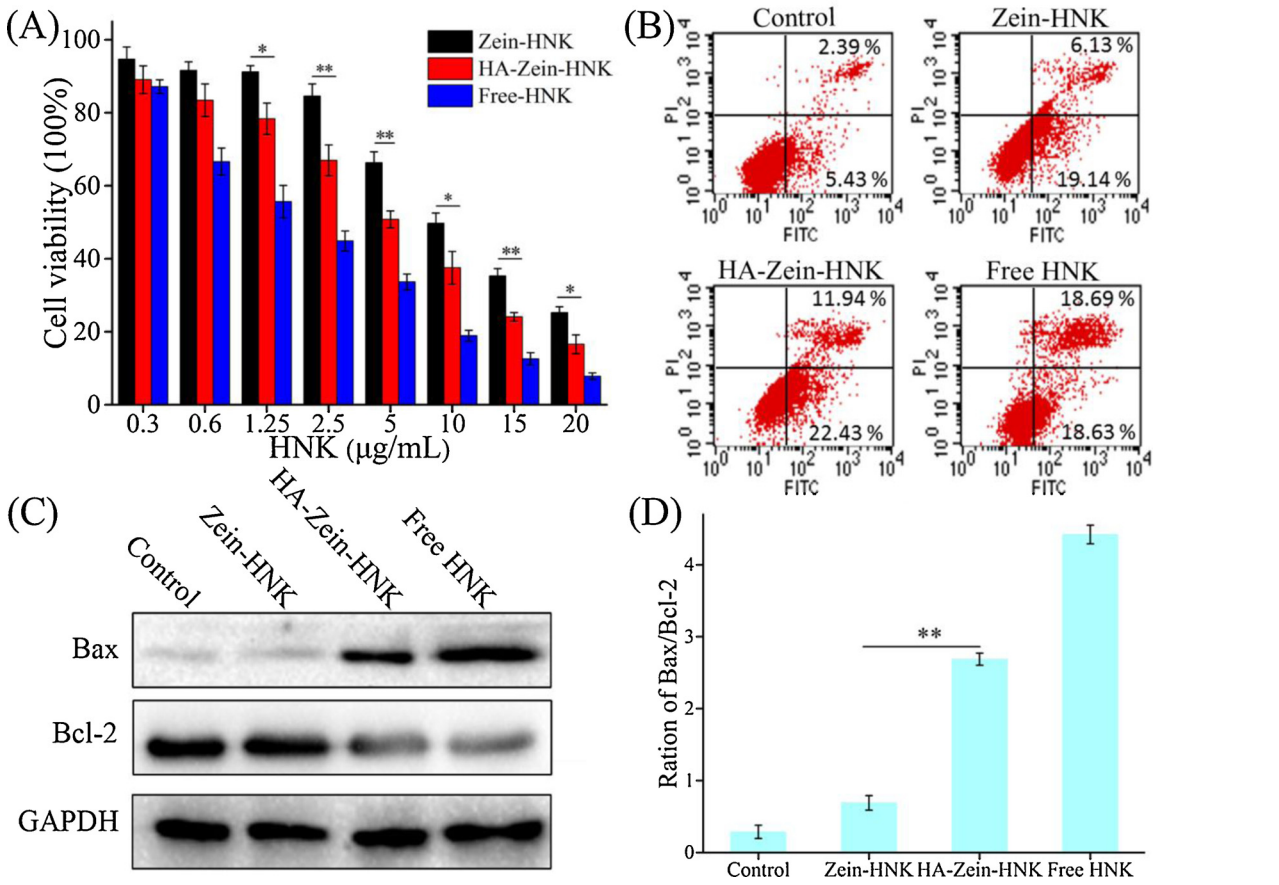

Fig. 3. *In vitro* efficacy evaluation of HA-Zein-HNK nanoparticles. (A) *In vitro* cytotoxicity evaluation of Zein-HNK, HA-Zein-HNK and free HNK in 4T1 cells for 48 h, data are presented as mean ± SD ($n = 6$), $^{*}p < 0.05$, $^{**}p < 0.01$. (B) *In vitro* cell apoptosis evaluation of Zein-HNK, HA-Zein-HNK and free HNK in 4T1 cells by flow cytometry. (C) Expressions of pro-apoptotic proteins Bax and anti-apoptotic proteins Bcl-2 in 4T1 cells incubation with various HNK formulatios. (D) The quantitative ration of Bax/Bcl-2 was calculated according to the band intensity in each group, $^{**}p < 0.01$.

enter cells *via* passive diffusion and be effective, whereas the HNK-loaded nanoparticles were mainly taken up by cells *via* the endocytic pathway and then the drug must be released to exert antitumor activity (Zhu et al., 2017). As expected, HA coating significantly increased the cytotoxicity of HNK-loaded zein nanoparticles at a concentration range of 1.25–20 μg/mL for the tested 4T1 cells. Furthermore, the cell populations at four different stages including dead cells, late apoptosis, early apoptosis and live cells were measured by flow cytometry after staining with the Annexin V-FITC/PI. Similar results were obtained in the cell apoptosis for 24 h treatment with Zein-HNK, HA-Zein-HNK and free HNK (Fig. 3B). The percentages of apoptotic cells in the control, Zein-HNK, HA-Zein-HNK and free HNK were 7.82 ± 0.64 %, 25.27 ± 0.85 %, 34.37 ± 1.48 % and 37.32 ± 2.61 %, respectively. In comparison to Zein-HNK, treating cells with HA-Zein-HNK significantly increased the ratio of apoptosis, which was in accordance with cytotoxicity results.

To further elucidate the apoptosis-inducing mechanism of HA-Zein-HNK, the protein expressions of the Bcl-2 and Bax in the 4T1 cells were analyzed by Western blotting. The members of the Bcl-2 family, as major cell survival and cell death regulators, were the main way to regulate the signaling pathway of mitochondria apoptosis (Hematpoor et al., 2018). The Bcl-2 acts as an anti-apoptotic protein, while Bax acts as a pro-apoptotic protein, and the balance of Bcl-2 and Bax is closely associated with apoptosis (Del Poeta et al., 2003). Thus, the ratio of Bax/Bcl-2 was usually used as an indicator for cell fate. According to Fig. 3C and D, compared to the control group, the level of Bcl-2 was down-regulated and the level of Bax was up-regulated when applying Zein-HNK, HA-Zein-HNK and free HNK. The increase of Bax activity in HA-Zein-HNK group was evidently higher than Zein-HNK, indicating the higher effect of HA-Zein-HNK on inducing cell apoptosis. These findings revealed that the enhancement of apoptosis in 4T1 cells following HA-Zein-HNK treatment was associated with the activation and regulation of the mitochondrion signaling apoptosis pathway.

3.4. *In vitro cell migration and invasion test*

Metastasis requires tumor cell dissemination to different organs from the primary tumor, and cell migration and invasion are two key procedures for this kind of dissemination (Bravo-Cordero, Hodgson, & Condeelis, 2012). Thus, cancer cell migration and invasion are directly related to metastasis (Cao et al., 2015). To evaluate the inhibitory effect of HA-Zein-HNK on cell mobility and invasion abilities, wound healing and transwell migration and invasion assays were performed. The cell motility was first estimated by wound healing assay. As shown in Fig. 4A and B, cells of the control group presented strong migration ability with most of wound healing at 24 h after scratched, indicating a high metastatic potential of 4T1 cells. And as a positive control, the free HNK showed the highest inhibition of cell motility with only 21.5 % of the wound healing rate. For Zein-HNK and HA-Zein-HNK treatments, the wound healing rates were 55.4 % and 29.2 %, respectively. This indicated that the migration inhibitory effect of HA-Zein-HNK was significantly stronger than that of Zein-HNK. The stronger inhibitory effects of HA-Zein-HNK could be owing to the HA coating, which remarkably increased the selective uptake of HA-Zein-HNK by 4T1 cells through the HA/CD44 receptor mediated endocytosis pathway.

The same results were observed in the corresponding transwell migration and invasion experiments (Fig. 4A, C and D). Compared to Zein-HNK treatment, lower cell migration and invasion rates for 4T1

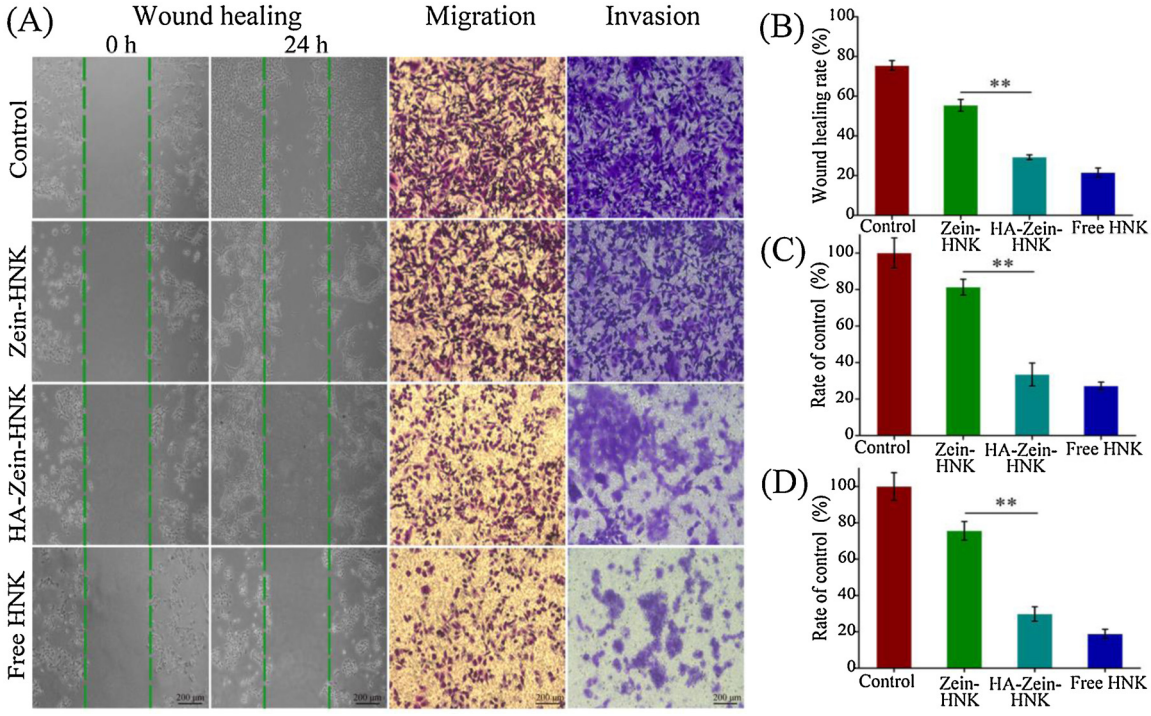

Fig. 4. *In vitro* inhibitory effects of Zein-HNK, HA-Zein-HNK and free HNK on cell migration and invasion abilities of 4T1 cells. (A) Typical optical images of wound healing, migration and invasion assessments of Zein-HNK, HA-Zein-HNK and free HNK in 4T1 cells. (B) Quantified wound healing inhibitory effect in comparison with negative control (**$p < 0.01$). (C) The percentage of migration cells were quantified and normalized by control group (**$p < 0.01$). (D) The percentage of invasion cells were quantified and normalized by control group (**$p < 0.01$).

cells were found in HA-Zein-HNK treatment. The migrated and invaded cells across the transwell membrane in the HA-Zein-HNK group were only 33.4 % and 29.8 % of the negative control. However, these rates unexpectedly increased to 81.3 % and 75.6 % in the Zein-HNK group. Thereby, the migration and invasion capacities of metastatic 4T1 cells could be significantly reduced by HA-Zein-HNK.

To further explore the anti-migration mechanism of HA-Zein-HNK, expressions of epithelial mesenchymal transition (EMT) associated markers including Vimentin and E-cadherin were determined by Western blotting. EMT is closely associated with the invasion and metastasis of many epithelial-derived tumors including breast cancer. Vimentin plays a major role in the alteration in shape, adhesion, and motility of the cells during EMT (He et al., 2020). While E-cadherin is an adhesion molecule that mediates cell adhesion of homogeneity, it is an important negative signal of EMT and its presence could reduce the metastatic ability of cells (Saadat et al., 2019). As shown in Fig. 5, all HNK formulations significantly upregulated E-cadherin (an epithelial marker) and downregulated Vimentin (a mesenchymal marker). E-cadherin was upregulated to 4.2 fold in the HA-Zein-HNK treated cells while there was 2.1 fold upregulation in Zein-HNK treatment. Moreover, there were 2.3 and 1.6 folds downregulation in Vimentin expression in the HA-Zein-HNK and Zein-HNK treated cells, respectively. The above results demonstrated that HA-Zein-HNK can inhibit cell migration and invasion by regulating the expression of E-cadherin and Vimentin in 4T1 cells.

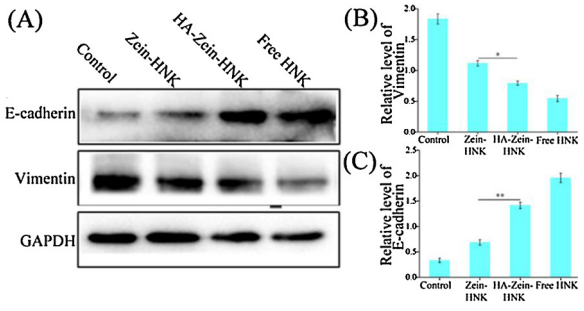

Fig. 5. (A) The expressions of Vimentin and E-cadherin in 4T1 cells treated by Zein-HNK, HA-Zein-HNK and free HNK were examined using western blot. GAPDH was used as internal control. (B and C) Analytic results of the band intensity values of Vimentin and E-cadherin, *$p < 0.05$ and **$p < 0.01$.

3.5. Inhibitory effect on the tumor spheroids

Tumor spheroids grown in 3D are an intermediate between monolayer cultures and *in vivo* studies (Friedrich, Seidel, Ebner, & Kunz-Schughart, 2009). They have been widely exploited in drug delivery system research for comprehensive study of drug efficacy, drug penetration, receptor targeting, and cell recruitment abilities (Huang & Gao, 2018). Thus, the inhibition of various HNK formulations on 3D tumor spheroids was investigated here. As shown in Fig. 6A and B, on the 4th day, the tumor spheroid volume ratios for the control were 285.7 ± 10.9 %, displaying the uncontrolled growth of tumor spheroids. Zein-HNK could reduce the volume to 36.1 ± 2.4 % at day 4, which was obviously lower than that of control. HA-Zein-HNK could be more effective to reduce the volume of tumor spheroids, which was 15.4 ± 2.2 % on day 4 after treatment, implying a better inhibitory effect of HA-Zein-HNK. The tumor spheroids growth inhibition results of various HNK formulations were similar with cytotoxicity results, indicating the better inhibition effect of HA-Zein-HNK was owing to the HA coating which could inhibit proliferation of not only the 2D monolayer cells but also the interior cells of 3D spheroids. These results gave straightforward evidence that the HA-Zein-HNK nanoparticles may be overcome the obstacle of inadequate drug amount into the inner of solid tumor that led to chemotherapy failure.

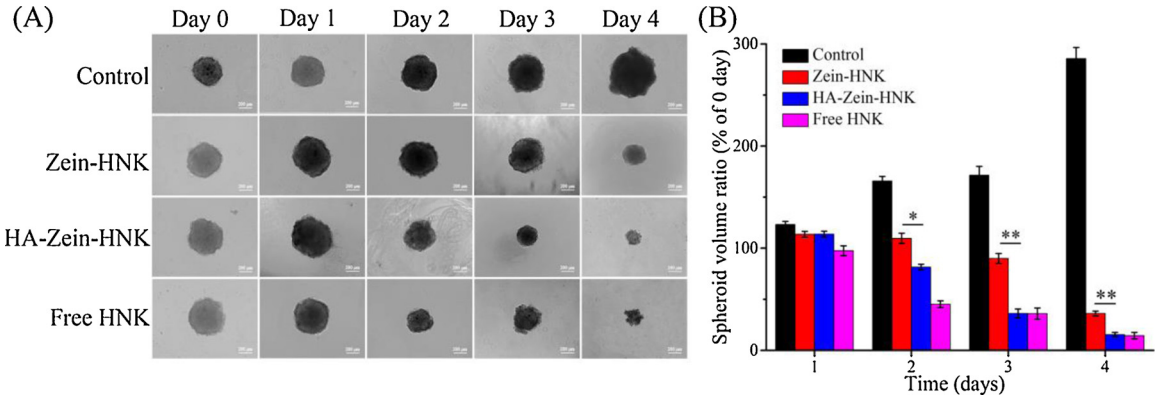

Fig. 6. *In vitro* inhibitory effect on 4T1 tumor spheroids. (A) Morphological change in 4T1 tumor spheroids during 4 days treatment with Zein-HNK, HA-Zein-HNK and free HNK (10 μg/mL). (B) The quantified size change of 4T1 tumor spheroids after treatment. Data are presented as the mean ± SD ($n = 3$), *$p < 0.05$ and **$p < 0.01$.

3.6. *In vivo* tissue distribution of DiR-loaded HA-Zein nanoparticles by living imaging

Recently, more and more attention has been paid to the utilization of fluorescent dyes to track the distribution passage of nanoparticles *in vivo*. Herein, to further verify the targeting capability of HA coating zein nanoparticles, the *in vivo* tissue distribution of the DiR loaded nanoparticles were tested on 4T1 tumor-bearing mice using a living fluorescence imaging system. Fig. 7A and C indicate apparent tumor and organ accumulations after the administration of Zein-DiR and HA-Zein-DiR. The fluorescence signal of tumor from HA-Zein-DiR was already evident as early as 12 h post administration, and the signal intensity was still high until the end of experiment at 48 h. While the fluorescence signal of Zein-DiR in tumor began to be obvious until 28 h post administration and was much weaker than that of HA-Zein-DiR during the whole tested time range. Due to the presence of HA coating in the HA-Zein-DiR nanoparticles, the accumulation of HA-Zein-DiR in the tumor was improved very well as there was obvious difference in the DiR fluorescence signals. In addition, the tumor and major organs were excised and imaged at the end of experiment (Fig. 7B and D), the HA-Zein-DiR treatment obtained higher intratumoral delivery and distributed more extensively within the tumor sites. Thus, this improved tissue distribution of the developed zein/HA core-shell nanoparticles would be highly beneficial for enhancing the therapeutic efficacy of antitumor agents such as HNK. Notably, the DiR accumulation in the lung was prominent for both the Zein-DiR and HA-Zein-DiR groups.

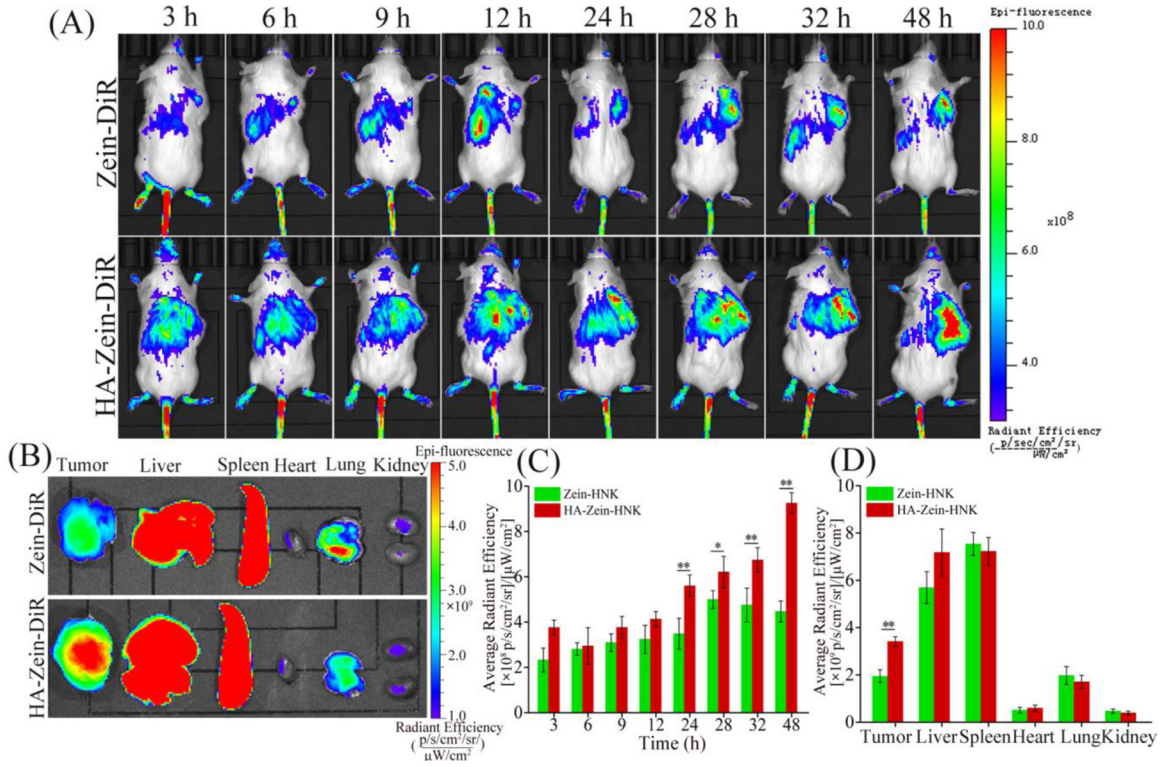

Fig. 7. *In vivo* biodistribution studies of different DiR loaded nanoparticles. (A) *In vivo* fluorescence images of 4T1 breast tumor-bearing BALB/c mice at different time points following injection of Zein-DiR and HA-Zein-DiR nanoparticles. (B) *Ex vivo* fluorescence images of tumors and organs after the mice were sacrificed at 48 h. (C) The semi-quantitative results of the *in vivo* fluorescent intensity of Zein-DiR and HA-Zein-DiR at different experimental time points. (D) The semi-quantitative results of the *ex vivo* fluorescent intensity of Zein-DiR and HA-Zein-DiR in major organs and tumors. Data are presented as the mean ± SD ($n = 3$), *$p < 0.05$ and **$p < 0.01$.

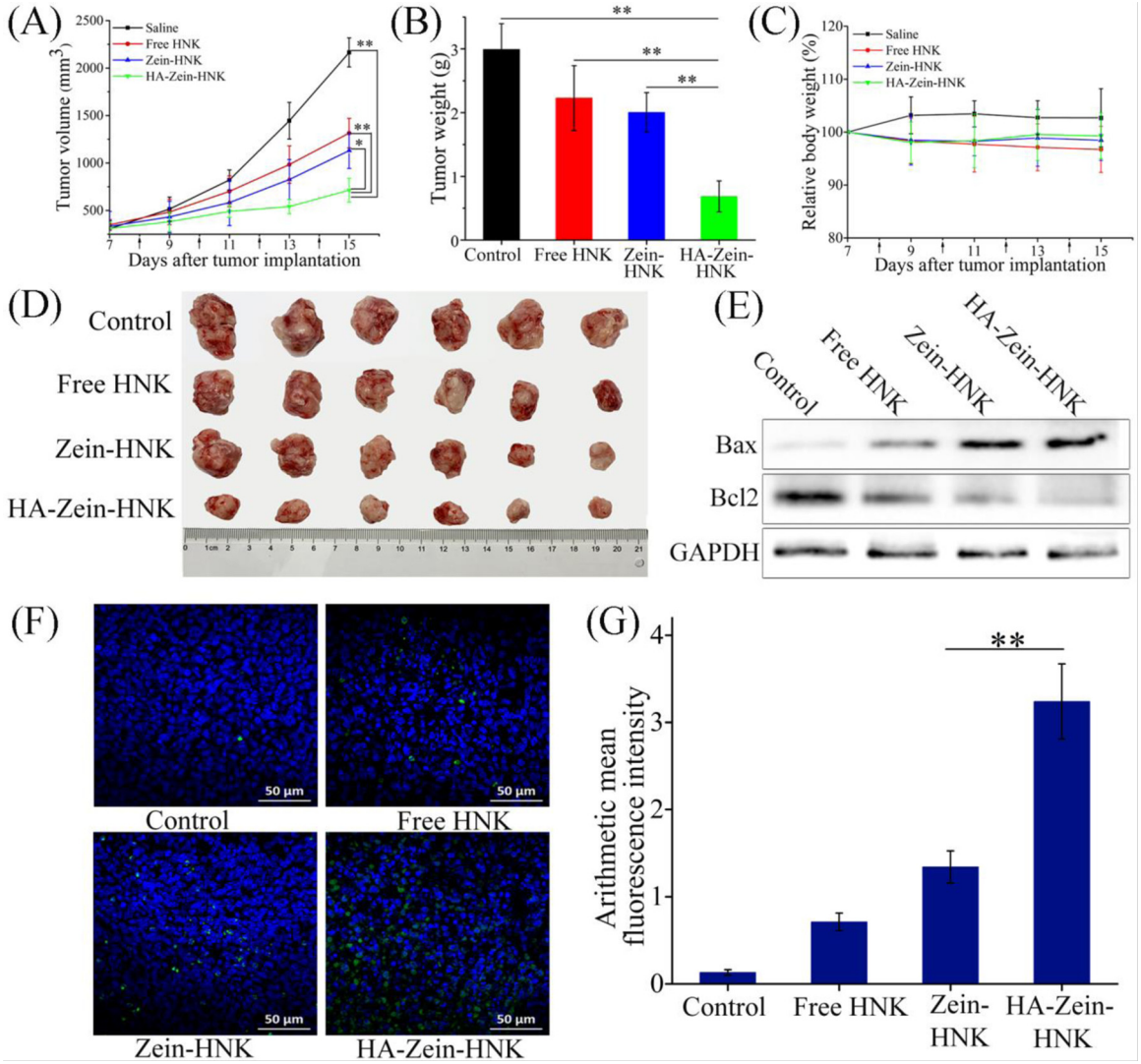

Fig. 8. Antitumor therapy activity of free HNK, Zein-HNK and HA-Zein-HNK in the BALB/c mice bearing 4T1 tumors at a dose of HNK 15 mg/kg, each formulation was intravenously administered every 2 days for a total of 4 times. (A) Tumor volume growth curves in different treatment groups. (B) The quantitative results of excised tumor weight in different treatment groups. (C) Variation in the net body weight of mice. (D) The photographs of the tumors in different treatment groups at the end of the experiment. (E) The expressions of Bax and Bcl-2 in tumor from each group. (F) The TUNEL examination of tumor sections. (G) The semi-quantitative results of TUNEL examination. Data were given as mean ± SD ($n = 6$). * $p < 0.05$ and ** $p < 0.01$.

And the DiR signal in Zein-DiR was much higher than that of the HA-Zein-DiR. This may be attributed to that airways and alveolar macrophages in the lung will selectively phagocytose particles larger than 100 nm. And nanoparticles tend to agglomerate due to interparticle ions in the aqueous airways where nanoparticles meet alveolar macrophages will compress the electrical double layer on the nanoparticles surface, leading to further agglomeration (Wang, He, Zhang, Zhao, & Feng, 2013; Yu et al., 2020). Moreover, nanoparticles with high cationic charge density show aggregation in the microvasculature of some organs such as liver, spleen and especially the lung (Saadat et al., 2019).

3.7. In Vivo therapeutic efficacy and toxicity studies

The *in vivo* therapeutic efficacy of HA-Zein-HNK was evaluated in BALB/c mice bearing 4T1 tumors and compared to physiological saline, free HNK and Zein-HNK treated mice. As shown in Fig. 8A, all HNK formulations displayed significant antitumor effects *in vivo* in comparison with physiological saline. As expected, HA-Zein-HNK generated a superior antitumor efficacy than free HNK and Zein-HNK, attributed to the active targeting effect of HA to CD44. After 4 times of HNK treatment, the tumors were dissected to measure their weights to further determine the therapeutic efficacy. The HA-Zein-HNK greatly reduced the tumor weight than the other treatments as shown in Fig. 8B and D. In agreement with the tumor volume measurement results, HA-Zein-HNK achieved the highest tumor weight inhibition (77.3%), followed by Zein-HNK (33 %) and free HNK (25.8 %). Up-regulation of pro-apoptotic Bax and down-regulation of anti-apoptotic Bcl2 (Fig. 8E) in all HNK formulations further confirmed the involvement of mitochondrion apoptosis pathway underlying antitumor effect *in vivo*. However, unlike *in vitro* results, where free HNK possessed the strongest modulated effect on the Bax/Bcl-2 ratio, HA-Zein-HNK presented the maximum *in vivo* modulation for the Bax/Bcl-2 ratio. It has been reported that HNK was usually used in combination with other chemotherapeutic agents to suppress vasculogenic mimicry, multidrug resistance and metastasis of breast cancer (Ju et al., 2018; Wang et al., 2017; Zou et al., 2018). The recent studies indicated that HNK used as a single agent required high doses(> 40 mg/kg) to produce significant anticancer activity against metastatic breast cancer (Wang et al., 2019; Yu et al., 2019). However, in this work, after encapsulating of HNK into

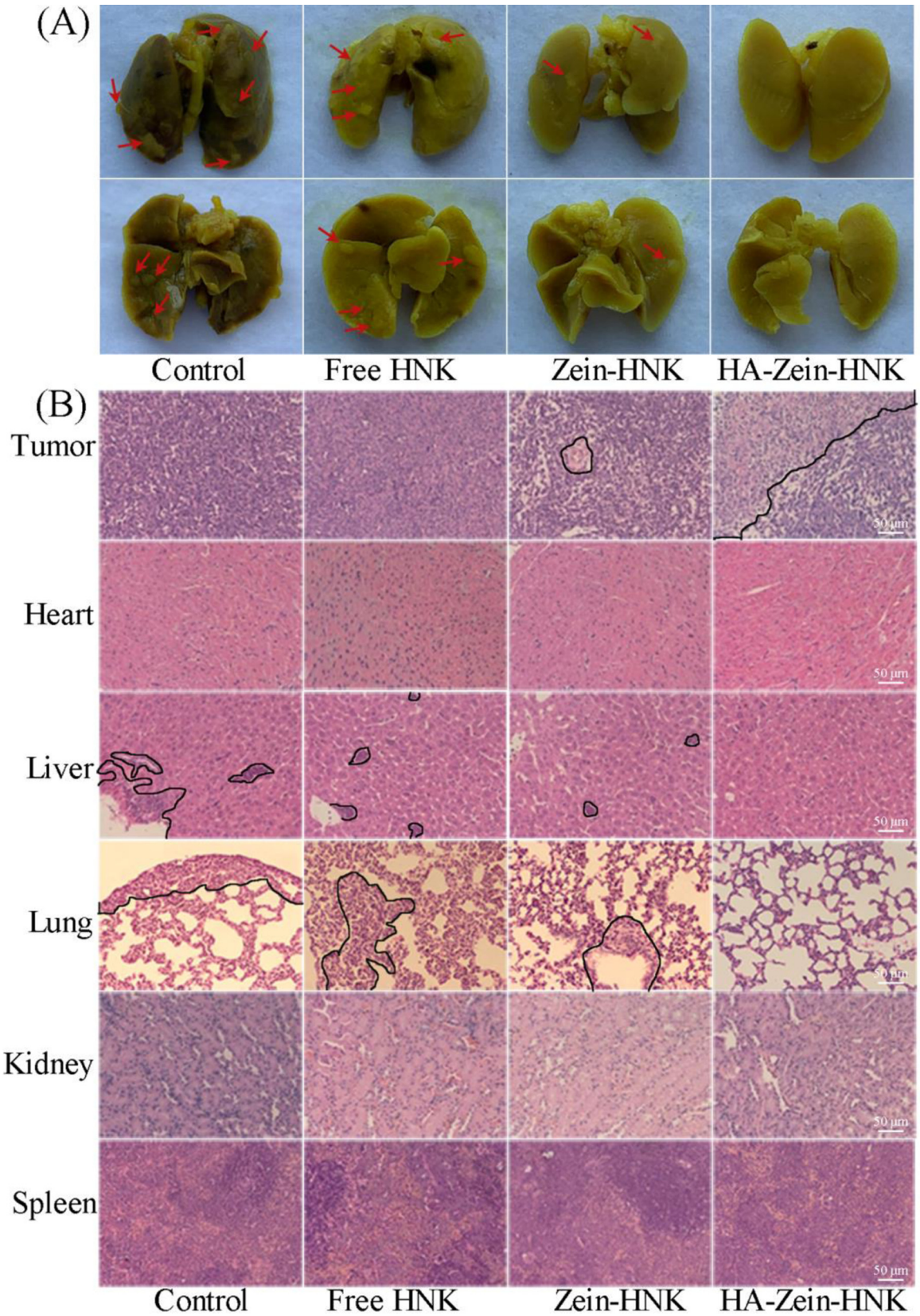

Fig. 9. (A) Representative images of pulmonary metastatic nodules (red arrows) of 4T1 tumor-bearing mice treated with free HNK, Zein-HNK and HA-Zein-HNK. (B) The histopathologic examination of the tumors and main organs after treatment by HE staining. The metastasis lesions were circled by black lines. (For interpretation of the references to colour in this figure legend, the reader is referred to the web version of this article).

zein/hyaluronic acid core-shell nanoparticles, the HNK's *in vivo* therapeutic efficacy was obviously improved even at a low dose (15 mg/kg), as confirmed by the excellent tumor volume and weight inhibitions. Moreover, results from H&E staining (Fig. 9B) and TUNEL labeling assay (Fig. 8F and G) clearly displayed significant cell death/necrosis and the highest degree of tumor apoptosis in HA-Zein-HNK group. Overall, these data confirmed the potential of HA-Zein-HNK on tumor growth inhibition.

In addition, the systemic toxicities of various HNK formulations were also evaluated. During the whole treatment period, no noticeable changes in the body weight of mice were observed (Fig. 8C). The H&E staining (Fig. 9B) indicated that no obvious organ damage was found after various HNK formulations treatments, which further verified the higher tolerance of HNK than other chemotherapy agents (Banik et al., 2019).

Metastasis usually occurs in the advanced stage of breast cancer. And approximately 25 % of breast cancer cases would succumb to their disease due to the progression and development of distant metastases in the lung, liver, brain and bone (Kaushal et al., 2018). Thus, the *in vivo* therapeutic efficacy of HA-Zein-HNK on metastasis of breast cancer was investigated. As shown in Fig. 9A, treatment with free HNK and Zein-HNK resulted in a decreased number of surface lung metastatic nodules compared to the physiological saline group, but the difference was not sufficiently distinctive. However, the treatment with HA-Zein-HNK showed the highest antimetastatic activity, as evidenced by hardly visible metastasis nodule. In addition, the histopathological analysis of the lung and liver tissues was performed by H&E staining to further validate the capacity of HA-Zein-HNK on inhibiting tumor metastasis (Fig. 9B). H&E staining of the lung and liver sections revealed that the number of metastases in the lung and liver closely related to the number of pulmonary surface lesions. And no metastasis was detected in the lung and liver of the mice treated with HA-Zein-HNK. Taken all together, the HNK loaded zein/hyaluronic acid core-shell nanoparticles display significant improvement in anticancer and antimetastasis efficacies while maintaining slight side effects.

The superior inhibition of HA-Zein-HNK on growth and metastasis of breast cancer could be attributed to the vast improvement of intracellular uptake efficiency, obvious enhancement of HNK concentration in the tumor sites and effective modulation of Bax and Bcl-2 expression ratio on breast cancer cells by the targeted nanocomplex. Additionally, the potent regulation of epithelial to mesenchymal transition (EMT) property of HNK could also play a significant role as the EMT was closely engaged in cancer invasion and metastasis (Wang, Yin et al., 2020; Yang & Weinberg, 2008). Therefore, the nanocomplex of HA-Zein-HNK could upgrade the therapeutic efficacy of HNK on metastatic breast cancer.

4. Conclusion

In this study, HA coated zein core-shell nanoparticles were successfully prepared to achieve targeted delivery of HNK to 4T1 breast cancer cells overexpressed CD44. HA-Zein-HNK exhibited remarkable characteristics including appropriate size and charge, high encapsulation efficiency, more stability and sustained release profile, rendering it suitable to be an efficient drug delivery system. The HA-Zein-HNK displayed significantly enhanced intracellular uptake efficiency, cytotoxicity, and pro-apoptotic activities *in vitro* as compared to Zein-HNK, owing to the presence of CD44 receptor mediated endocytosis. More importantly, HA-Zein-HNK showed remarkable anti-invasion and anti-migration effects on tumor cell through the regulation of EMT related proteins expression. As a consequence, the HA-Zein-HNK exhibited enhanced antitumor and antimetastasis efficacies *in vivo* with no obvious systemic toxicity for the treatment of aggressive breast cancer in mouse models. Therefore, the HA-Zein-HNK reported here was verified as a promising strategy for inhibiting growth and metastasis of breast cancer.

CRediT authorship contribution statement

Qi Zhang: Investigation, Writing - original draft, Visualization, Funding acquisition. **Jing Wang:** Investigation, Validation. **Dan Liu:** Validation. **Wenquan Zhu:** Formal analysis, Validation. **Shuang Guan:** Visualization, Methodology. **Li Fan:** Methodology. **Defu Cai:** Writing - review & editing, Supervision, Visualization, Project administration, Resources, Funding acquisition.

Declaration of Competing Interest

The authors declare no conflict of interest.

Acknowledgments

This work was financially supported by National Natural Science Foundation of China (grant numbers 81873172, 81650021), China Postdoctoral Science Foundation (grant number 2019M661321), Scientific Research Fund of Qiqihar Academy of Medical Sciences, China (grant numbers QMSI2017LX-01, QMSI2017LX-02) and Scientific Research Fund of Heilongjiang Provincial Education Department, China (grant number 2018-KYYWF-0081).

References

Banik, K., Ranaware, A. M., Deshpande, V., Nalawade, S. P., Padmavathi, G., Bordoloi, D., ... Kunnumakkar, A. B. (2019). Honokiol for cancer therapeutics: A traditional medicine that can modulate multiple oncogenic targets. *Pharmacological Research, 144*, 192–209.

Bravo-Cordero, J. J., Hodgson, L., & Condeelis, J. (2012). Directed cell invasion and migration during metastasis. *Current Opinion in Cell Biology, 24*(2), 277–283.

Cao, H. Q., Zhang, Z. W., Zhao, S., He, X. Y., Yu, H. J., Yin, Q., ... Li, Y. P. (2015). Hydrophobic interaction mediating self-assembled nanoparticles of succinobucol suppress lung metastasis of breast cancer by inhibition of VCAM-1 expression. *Journal of Controlled Release, 205*, 162–171.

Chen, D. H., Sun, Y. T., Wei, Y. K., Zhang, P. J., Rezaeian, A. H., Teruya-Feldstein, J., ... Ma, L. (2012). LIFR is a breast cancer metastasis suppressor upstream of the Hippo-YAP pathway and a prognostic marker. *Nature Medicine, 18*(10), 1511–U1105.

Chen, S., Han, Y. H., Huang, J. Y., Dai, L., Du, J., McClements, D. J., ... Gao, Y. X. (2019). Fabrication and characterization of layer-by-Layer composite nanoparticles based on Zein and hyaluronic acid for codelivery of curcumin and quercetagetin. *ACS Applied Materials & Interfaces, 11*(18), 16922–16933.

Chen, S., Han, Y. H., Wang, Y. Q., Yang, X., Sun, C. X., Mao, L. K., ... Gao, Y. X. (2019). Zein-hyaluronic acid binary complex as a delivery vehicle of quercetagetin: Fabrication, structural characterization, physicochemical stability and in vitro release property. *Food Chemistry, 276*, 322–332.

Chiu, C. S., Tsai, C. H., Hsieh, M. S., Tsai, S. C., Jan, Y. J., Lin, W. Y., ... Sheu, M. L. (2019). Exploiting honokiol-induced ER stress CHOP activation inhibits the growth and metastasis of melanoma by suppressing the MITF and beta-catenin pathways. *Cancer Letters, 442*, 113–125.

Del Duca, D., Werbowetski, T., & Del Maestro, R. F. (2004). Spheroid preparation from hanging drops: Characterization of a model of brain tumor invasion. *Journal of Neuro-oncology, 67*(3), 295–303.

Del Poeta, G., Venditti, A., Del Principe, M. I., Maurillo, L., Buccisano, F., Tamburini, A., ... Amadori, S. (2003). Amount of spontaneous apoptosis detected by Bax/Bcl-2 ratio predicts outcome in acute myeloid leukemia (AML). *Blood, 101*(6), 2125–2131.

Dicker, K. T., Gurski, L. A., Pradhan-Bhatt, S., Witt, R. L., Farach-Carson, M. C., & Jia, X. Q. (2014). Hyaluronan: A simple polysaccharide with diverse biological functions. *Acta Biomaterialia, 10*(4), 1558–1570.

Dosio, F., Arpicco, S., Stella, B., & Fattal, E. (2016). Hyaluronic acid for anticancer drug and nucleic acid delivery. *Advanced Drug Delivery Reviews, 97*, 204–236.

Friedrich, J., Seidel, C., Ebner, R., & Kunz-Schughart, L. A. (2009). Spheroid-based drug screen: Considerations and practical approach. *Nature Protocols, 4*(3), 309–324.

Ganesh, S., Iyer, A. K., Morrissey, D. V., & Amiji, M. M. (2013). Hyaluronic acid based self-assembling nanosystems for CD44 target mediated siRNA delivery to solid tumors. *Biomaterials, 34*(13), 3489–3502.

He, Y., Hou, X., Guo, J., He, Z., Guo, T., Liu, Y., ... Feng, N. (2020). Activation of a gamma–cyclodextrin–based metal–organic framework using supercritical carbon dioxide for high–efficient delivery of honokiol. *Carbohydrate Polymers, 235*, 115935.

Hematpoor, A., Paydar, M., Liew, S. Y., Sivasothy, Y., Mohebali, N., Looi, C. Y., ... Awang, K. (2018). Phenylpropanoids isolated from Piper sarmentosum Roxb. induce apoptosis in breast cancer cells through reactive oxygen species and mitochondrial-dependent pathways. *Chemico-biological Interactions, 279*, 210–218.

Hu, K., & McClements, D. J. (2015). Fabrication of biopolymer nanoparticles by anti-solvent precipitation and electrostatic deposition: Zein-alginate core/shell nanoparticles. *Food Hydrocolloids, 44*, 101–108.

Huang, B. W., & Gao, J. Q. (2018). Application of 3D cultured multicellular spheroid tumor models in tumor-targeted drug delivery system research. *Journal of Controlled*

Release, 270, 246–259.
Jiang, Y., Zhang, C., Yuan, J. H., Wu, Y. Y., Li, F., Li, D. P., ... Huang, Q. R. (2019). Effects of pectin polydispersity on zein/pectin composite nanoparticles (ZAPs) as high internal-phase pickering emulsion stabilizers. *Carbohydrate Polymers, 219*, 77–86.
Ju, R. J., Cheng, L., Qiu, X., Liu, S., Song, X. L., Peng, X. M., ... Li, X. T. (2018). Hyaluronic acid modified daunorubicin plus honokiol cationic liposomes for the treatment of breast cancer along with the elimination vasculogenic mimicry channels. *Journal of Drug Targeting, 26*(9), 793–805.
Kaushal, N., Tiruchinapally, G., Durmaz, Y. Y., Bao, L. W., Gilani, R., Merajver, S. D., ... ElSayed, M. E. H. (2018). Synergistic inhibition of aggressive breast cancer cell migration and invasion by cytoplasmic delivery of anti-RhoC silencing RNA and presentation of EPPT1 peptide on "smart" particles. *Journal of Controlled Release, 289*, 79–93.
Kaushik, P., Rawat, K., Aswal, V. K., Kohlbrecher, J., & Bohidar, H. B. (2019). Fluorescent complex coacervates of agar and in situ formed zein nanoparticles: Role of electrostatic forces. *Carbohydrate Polymers, 224*, 115150.
Lang, T. Q., Dong, X. Y., Huang, Y., Ran, W., Yin, Q., Zhang, P. C., ... Li, Y. P. (2017). Ly6C(hi) monocytes delivering pH-Sensitive micelle loading paclitaxel improve targeting therapy of metastatic breast cancer. *Advanced Functional Materials, 27*(26), 1701093.
Li, H., Xu, Y., Sun, X., Wang, S. H., Wang, J. W., Zhu, J. X., ... Zhao, L. L. (2018). Stability, bioactivity, and bioaccessibility of fucoxanthin in zein-caseinate composite nanoparticles fabricated at neutral pH by antisolvent precipitation. *Food Hydrocolloids, 84*, 379–388.
Liang, D. S., Zhang, W. J., Wang, A. T., Su, H. T., Zhong, H. J., & Qi, X. R. (2017). Treating metastatic triple negative breast cancer with CD44/neuropilin dual molecular targets of multifunctional nanoparticles. *Biomaterials, 137*, 23–36.
Lv, X. Q., Qiao, X. R., Su, L., & Chen, S. Z. (2016). Honokiol inhibits EMT-mediated motility and migration of human non-small cell lung cancer cells in vitro by targeting c-FLIP. *Acta Pharmacologica Sinica, 37*(12), 1574–1586.
Peer, D., & Margalit, R. (2004). Tumor-targeted hyaluronan nanoliposomes increase the antitumor activity of liposomal Doxorubicin in syngeneic and human xenograft mouse tumor models. *Neoplasia, 6*(4), 343–353.
Pulakkat, S., Balaji, S. A., Rangarajan, A., & Raichur, A. M. (2016). Surface engineered protein nanoparticles with hyaluronic acid based multilayers for targeted delivery of anticancer agents. *ACS Applied Materials & Interfaces, 8*(36), 23437–23449.
Ravar, F., Saadat, E., Gholami, M., Dehghankelishadi, P., Mahdavi, M., Azami, S., ... Dorkoosh, F. A. (2016). Hyaluronic acid-coated liposomes for targeted delivery of paclitaxel, in-vitro characterization and in-vivo evaluation. *Journal of Controlled Release, 229*, 10–22.
Saadat, M., Zahednezhad, F., Zakeri-Milani, P., Heidari, H. R., Shahbazi-Mojarrad, J., & Valizadeh, H. (2019). Drug targeting strategies based on charge dependent uptake of nanoparticles into cancer cells. *Journal of Pharmacy & Pharmaceutical Sciences, 22*, 191–220.
Seok, H. Y., Rejinold, N. S., Lekshmi, K. M., Cherukula, K., Park, I. K., & Kim, Y. C. (2018). CD44 targeting biocompatible and biodegradable hyaluronic acid cross-linked zein nanogels for curcumin delivery to cancer cells: In vitro and in vivo evaluation. *Journal of Controlled Release, 280*, 20–30.
Sheikhi, A., Hayashi, J., Eichenbaum, J., Gutin, M., Kuntjoro, N., Khorsandi, D., ... Khademhosseini, A. (2019). Recent advances in nanoengineering cellulose for cargo delivery. *Journal of Controlled Release, 294*, 53–76.
Siegel, R. L., Miller, K. D., & Jemal, A. (2019). Cancer statistics, 2019. *Ca-a Cancer Journal for Clinicians, 69*(1), 7–34.
Song, M. J., Liang, Y., Li, K. K., Zhang, J., Zhang, N., Tian, B. C., ... Han, J. T. (2019). Hyaluronic acid modified liposomes for targeted delivery of doxorubicin and paclitaxel to CD44 overexpressing tumor cells with improved dual-drugs synergistic effect. *Journal of Drug Delivery Science and Technology, 53*, 101179.
Tran, P. H. L., Dian, W., Lee, B. J., & Tran, T. T. D. (2019). The use of zein in the controlled release of poorly water-soluble drugs. *International Journal of Pharmaceutics, 566*, 557–564.
Wang, B., He, X., Zhang, Z. Y., Zhao, Y. L., & Feng, W. Y. (2013). Metabolism of nanomaterials in vivo: Blood circulation and organ clearance. *Accounts of Chemical Research, 46*(3), 761–769.
Wang, J., Liu, D., Guan, S., Zhu, W., Fan, L., Zhang, Q., ... Cai, D. (2020). Hyaluronic acid-modified liposomal honokiol nanocarrier: Enhance anti-metastasis and antitumor efficacy against breast cancer. *Carbohydrate Polymers, 235*, 115981.
Wang, W. D., Shang, Y., Li, Y., & Chen, S. Z. (2019). Honokiol inhibits breast cancer cell metastasis by blocking EMT through modulation of Snail/Slug protein translation. *Acta Pharmacologica Sinica, 40*(9), 1219–1227.
Wang, Y., Yin, S., Mei, L., Yang, Y., Xu, S., He, X., ... He, Q. (2020). A dual receptors-targeting and size-switchable “cluster bomb” co-loading chemotherapeutic and transient receptor potential ankyrin 1 (TRPA-1) inhibitor for treatment of triple negative breast cancer. *Journal of Controlled Release, 321*, 71–83.
Wang, Z. Q., Li, X. R., Wang, D. S., Zou, Y., Qu, X. Y., He, C. Y., ... Liu, Y. (2017). Concurrently suppressing multidrug resistance and metastasis of breast cancer by co-delivery of paclitaxel and honokiol with pH-sensitive polymeric micelles. *Acta Biomaterialia, 62*, 144–156.
Xu, G., Dong, R., Liu, J., Zhao, L., Zeng, Y., Xiao, X., ... Yang, T. (2019). Synthesis, characterization and in vivo evaluation of honokiol bisphosphate prodrugs protects against rats’ brain ischemia-reperfusion injury. *Asian Journal of Pharmaceutical Sciences, 14*(6), 640–648.
Yang, J., & Weinberg, R. A. (2008). Epithelial-mesenchymal transition: At the crossroads of development and tumor metastasis. *Developmental Cell, 14*(6), 818–829.
Yu, R. Q., Zou, Y., Liu, B. A., Guo, Y. F., Wang, X. T., & Han, M. H. (2019). Surface modification of pH-sensitive honokiol nanoparticles based on dopamine coating for targeted therapy of breast cancer. *Colloids and Surfaces B-Biointerfaces, 177*, 1–10.
Yu, X. L., Wu, H. C., Hu, H. Y., Dong, Z. Y., Dang, Y. N., Qi, Q., ... Lu, Y. (2020). Zein nanoparticles as nontoxic delivery system for maytansine in the treatment of non-small cell lung cancer. *Drug Delivery, 27*(1), 100–109.
Zhang, L., Su, H. T., Liu, Y. J., Pang, N., Li, J., & Qi, X. R. (2019). Enhancing solid tumor therapy with sequential delivery of dexamethasone and docetaxel engineered in a single carrier to overcome stromal resistance to drug delivery. *Journal of Controlled Release, 294*, 1–16.
Zhang, Y., Cui, L. L., Che, X. X., Zhang, H., Shi, N. Q., Li, C. L., ... Kong, W. (2015). Zein-based films and their usage for controlled delivery: Origin, classes and current landscape. *Journal of Controlled Release, 206*, 206–219.
Zhang, Y. X., Chen, T., Yuan, P., Tian, R., Hu, W. J., Tang, Y. L., ... Zhang, L. K. (2015). Encapsulation of honokiol into self-assembled pectin nanoparticles for drug delivery to HepG2 cells. *Carbohydrate Polymers, 133*, 31–38.
Zhang, Z. W., Cao, H. Q., Jiang, S. J., Liu, Z. Y., He, X. Y., Yu, H. J., ... Li, Y. P. (2014). Nanoassembly of probucol enables novel therapeutic efficacy in the suppression of lung metastasis of breast cancer. *Small, 10*(22), 4735–4745.
Zhu, D. W., Wu, S. J., Hu, C. Y., Chen, Z., Wang, H., Fan, F., ... Zhang, L. H. (2017). Folate-targeted polymersomes loaded with both paclitaxel and doxorubicin for the combination chemotherapy of hepatocellular carcinoma. *Acta Biomaterialia, 58*, 399–412.
Zou, Y., Zhou, Y. H., Jin, Y., He, C. Y., Deng, Y. Q., Han, S. D., ... Liu, Y. (2018). Synergistically enhanced antimetastasis effects by honokiol-loaded ph-sensitive polymer-doxorubicin conjugate micelles. *ACS Applied Materials & Interfaces, 10*(22), 18585–18600.